Applied Energy 318 (2022) 119245

Contents lists available at ScienceDirect

Applied Energy

journal homepage: www.elsevier.com/locate/apenergy

Co-optimization of repairs and dynamic network reconfiguration for improved distribution system resilience☆

Qingxin Shi [a], Fangxing Li [a,*], Jin Dong [b], Mohammed Olama [b], Xiaofei Wang [a], Chris Winstead [b], Teja Kuruganti [b]

[a] Department of Electrical Eng. & Computer Science, University of Tennessee, Knoxville, TN, USA
[b] Oak Ridge National Laboratory, Oak Ridge, TN, USA

HIGHLIGHTS

- A mathematically rigorous two-stage repair and restoration algorithm is proposed.
- The algorithm considers the coupling of repair, reconfiguration, and DER dispatch.
- The first stage determines the optimal repair sequence of faulted lines.
- The second stage re-dispatches the DER output based on the latest load consumption.

ARTICLE INFO

Keywords:
Resilience
Distribution system restoration
Repair crew
Network reconfiguration
Distributed energy resource (DER)

ABSTRACT

In this paper, a post-disaster distribution system repair and restoration (DSRR) strategy is proposed to improve distribution system resilience. The DSRR strategy is formulated as a two-stage optimization. The first stage is a comprehensive co-optimization of repair crew scheduling, dynamic network reconfiguration, and distributed energy resource (DER) dispatch based on the forecast load profile. The goal is to minimize the accumulative operating cost caused by the load reduction payment as well as DER operating cost. In particular, since the number of available repair crews is usually smaller than the number of faulted lines after a disaster event, the DSRR strategy determines the optimal scheduling for repairing faulted lines. The second stage is a re-dispatch of the DER power output and load shedding based on the real-time load demand of each bus. The proposed algorithm is validated by case studies of the IEEE 33-bus and 123-bus test systems. We consider those scenarios in which faults occur in multiple heavy-loaded feeders. The simulation results demonstrate that the DSRR strategy effectively coordinate the repair scheduling, network reconfiguration and load shedding to minimize the operating cost.

1. Introduction

Power system resilience is the grid's ability to withstand and rapidly recover from high-impact low-probability events, such as hurricanes, earthquakes, and deliberate threats [1–3]. A system-level power outage after an extreme event can cause significant inconvenience and economic loss to customers. For example, in 2017, power outages due to hurricanes Harvey, Irma, and Maria caused a total economic loss of around $202 billion in the U.S. [4]. It is essential for utilities to quickly restore the unserved load by making use of repair crews, normal-open tie lines, and distributed energy resources (DERs). The distribution system repair and restoration (DSRR) algorithm solves for this problem [5].

Previous works have been conducted on network reconfiguration

☆ This material is based upon work supported by the U.S. Department of Energy (DOE), Grid Modernization Laboratory Consortium (GMLC), DOE Office of Electricity, and Building Technologies Office. This manuscript has been authored by UT-Battelle, LLC under Contract No. DE-AC05-00OR22725 with the US Department of Energy. The United States Government retains and the publisher, by accepting the article for publication, acknowledges that the United States Government retains a non-exclusive, paid-up, irrevocable, worldwide license to publish or reproduce the published form of this manuscript, or allow others to do so, for United States Government purposes. The Department of Energy will provide public access to these results of federally sponsored research in accordance with the DOE Public Access Plan (https://energy.gov/downloads/doe-public-access-plan).

* Corresponding author.
E-mail address: fli6@utk.edu (F. Li).

https://doi.org/10.1016/j.apenergy.2022.119245
Received 19 October 2021; Received in revised form 11 April 2022; Accepted 2 May 2022
Available online 16 May 2022

Nomenclature

Operator

$\|.\|$	Dimension of a vector
$\lceil\rceil$	Rounding up sign
$(\widehat{x})$	The forecast value of parameter x

Indices and sets

t, Ω_T	Index and set of timeslots
j, Ω_N	Index and set of buses
$\Omega_{N,G} \subset \Omega_N$	Set of buses with fuel-based distributed generators (DGs)
$\Omega_{N,C} \subset \Omega_N$	Set of buses with shunt capacitors
$\Omega_{N,E} \subset \Omega_N$	Set of buses with battery energy storage system (BESS)
(i, j), Ω_B	Index and the set of lines
$\Omega_{B,Ns} \subset \Omega_B$	Set of lines without remote-controlled switch (RCS)
$\Omega_{B,Fa} \subset \Omega_B$	Set of faulted lines

Parameters

c^G	Operation cost of the fuel-based generator
c^L	Payment for load shedding
$\overline{T}_{ij}^{rep}$	Time consumption for reaching the faulted line (i, j) and repairing it
N^{rep}	Number of available line repair crews
N^{sw}	Maximal number of switch status change
$\delta(j)$ / $\pi(j)$	Set of child/parent buses of bus j
P_j^{Gmax}	Generator output upper limit at bus j
P_j^L	Daily peak load at bus j
$\widehat{P}_{j,t}^L/\widehat{Q}_{j,t}^L$	Real/reactive load demand at bus j, time t (forecast values)
$P_{j,t}^L/Q_{j,t}^L$	Real/reactive load demand at bus j, time t (practical values)
$Q_j^{C,rated}$	Rated reactive power output of capacitor j
R_{ij} / X_{ij}	Resistance/inductance of line (i, j)
S_{ij}^{max}	Thermal limit of line (i, j)
V^{max}/V^{min}	Maximal/minimal bus voltage
V_{sub}	Substation secondary voltage

Variables

$\nu_{ij,t}$	Repair state variable of line (i, j) at time t; 1 if being repaired by a crew, 0 otherwise
$y_{ij,t}$	Outage state variable line (i, j) at t; 1 if having been repaired, 0 otherwise
$\mu_{ij,t}$	Outage state change variable of line (i, j) at t; 1 if $y_{ij,t\text{-}1} = 0$ and $y_{ij,t} = 1$, 0 otherwise
$z_{ij,t}$	Switching state variable of non-faulted (or repaired) line (i, j); 1 if closed, 0 otherwise
$s_{ij,t}$	Binary variable indicating the state change of $z_{ij,t}$; 1 if $z_{ij,t\text{-}1} \neq y_{ij,t}$, 0 otherwise
F_{ij}	Power flow of line (i, j) in the virtual network
$P_{j,t}^G$	DG power output at bus j, time t
$\Delta P_{j,t}^L$	Load shedding at bus j, time t
$Q_{j,t}^C$	Reactive power output of the shunt capacitor at bus j, time t
$P_{j,t}^{Bdch}$	BESS discharging power at bus j, time t
$E_{j,t}^B$	BESS remaining energy at bus j, time t
$P_{ij,t}$ /$Q_{ij,t}$	Real/reactive power flow of line (i, j), time t
$V_{j,t}$	Voltage at bus j, time t

and DER scheduling for the resilient operation of distribution systems. One major approach is to split the on-outage part of the system into self-supplied microgrids [6–9]. The authors in [7] proposed a master–slave DER and network reconfiguration method to maximize the restored load. The study in [8] proposed a two-stage restoration strategy, in which the first stage determines the post-restoration topology and the second stage schedules the restored load. The study in [10] proposed a heuristic-searching-based radial constraint for post-disaster restoration. Overall, the above approaches were focused on network reconfiguration and DER scheduling. However, the restoration strategies in [6–10] neither considered the optimal repair crew scheduling nor made use of the repaired components until all of them are repaired. Hence, there is still room for reducing the operating cost in the DSRR period.

After a severe natural disaster, the number of faulted lines is usually larger than the number of repair crews, and the optimal sequence of repairing lines can lead to the largest amount of load to be restored in the DSRR period. Dispatching repair crews based on operators' experience may not lead to an optimal plan for post-disaster restoration. Hence, there is a need to develop a mathematically rigorous strategy to optimally coordinate repair crew scheduling, network reconfiguration, and DERs to minimize the post-disaster operating cost. In [11,12], a restoration framework was proposed to generate an optimal switching sequence after N-k line faults in the distribution system. However, the application scenario of this framework is a cascading failure rather than physical damage to distribution lines. Day-ahead pre-disaster restoration planning aims to minimize the operating cost by dispatching repair resources. The problem can be formulated as a two-stage stochastic programming problem [13] or a bi-level robust optimization problem [14] to address random scenarios. In recent years, the post-hurricane DSRR strategy has drawn much attention, as in [15]. Soft precedence constraints were introduced to mitigate the NP-hard problem and to improve computational efficiency. However, the DER dispatch was not considered in the restoration process. The study in [16] proposed a two-stage DSRR strategy. The first stage clustered repair tasks considering the traveling distance of crews, while the second stage co-optimized the repair crews, network reconfiguration, and DER dispatch based on the deterministic load demand. The study in [5] formulated the DSRR as a two-stage stochastic programming considering the uncertainty of repair time and load profile. The first stage finds the optimal sequence of repair crews, and the second stage completes service restoration using reconfiguration and DERs. The authors in [17] proposed a tri-stage DSRR strategy to handle the uncertainty of load profile and repair time. The study considers an unbalanced distribution system model and a more detailed crew model (e.g., line repair crew and tree removal crew) for the restoration. In fact, the two-stage stochastic optimization adopted in [5,17] is an effective approach to power system long-term planning problems, it is not necessarily applicable to operation problems for two reasons: 1) The solution of stochastic programming results in high computational workload, while the operation problem requires quick solution for dispatch action; 2) The two-stage formulation essentially solves for the expected optimal solution under all stochastic scenarios, while does not ensure optimal solution for a single scenario [20,21].

To summarize, repair crew scheduling is coupled with network reconfiguration and load shedding during the restoration process. Since the two dispatch behaviors involve many time-dependent constraints, they should be determined in the beginning to achieve a global optimization. This paper proposes a mathematically rigorous two-stage DSRR algorithm for improved resilience against hurricanes. By making full use of repair crews, switchable tie lines, and DERs, the algorithm can solve for a global optimal restoration with regard to N-k contingencies. The innovations of this paper are summarized as follows:

- The first stage of the DSRR strategy aims to determine the line repair sequence and dynamic network reconfiguration to minimize the system operating cost during the restoration period. A set of simple linear constraints is proposed to characterize the behavior of repair

crew dispatch. The method makes a good trade-off between accuracy and computational workload by simplifying crew routing constraints.
- Based on the optimal repair sequence and reconfiguration, the second stage is hourly re-dispatch of DGs and load shedding based on the latest load consumption at each bus. This approach mitigates the generation-load mismatch that is caused by the load/PV forecast error.

The rest of the paper is organized as follows. Section 2 introduces the application background of the distribution system restoration. Section 3 proposes the two-stage DSRR algorithm that determines the optimal repair sequence and the dynamic network reconfiguration. Section4 presents the numerical study results to validate the proposed algorithm. Finally, Section 5 concludes the paper and introduces future research directions.

2. Background of post-disaster restoration

The design of an optimal DSRR strategy largely depends on a detailed analysis of the application background, including the characteristics of the disaster, the distribution system infrastructure, and the routing features of repair crews.

2.1. Hurricane characteristics

The distribution system infrastructure is vulnerable to extreme weather events, especially hurricanes. Generally, coastal areas suffer the most severe damage in hurricane events [22,23]. The radial distribution of wind speed in a hurricane is shown in Fig. 1 [24]. The wind is strongest at the eyewall (at the distance of 22 km). The moving speed of a hurricane eye ranges from 20 to 30 km/hour. As a consequence, it may take a few hours for the hurricane eye to sweep over a distribution system. In consideration of safety, repair crews start working on the faulted lines only after the hurricane eye moves away and all the distribution system damages are identified. Therefore, it is reasonable to assume that the hurricane only does not cause further damage to a distribution system after the DSRR starts.

2.2. *Characteristics* of distribution system operation

The proposed DSRR strategy is based on the following assumptions with regard to the distribution system operation.

- The upstream transmission system normally operates in extreme weather. This assumption is based on the statistical data that 90% of the unscheduled line faults in the U.S. occur in distribution systems [25].
- The faulted line can be located by the fault indicator [17,26]. Also, some portions of lines in the distribution system are equipped with remote-controlled switches (RCSs) that can receive control signals from the distribution system operator (DSO) [28]. The DSO is able to control the load of each bus.
- The battery energy storage system (BESS) and fuel-based DG operate at unity power factor and, thus, do not participate in volt-var control [27].

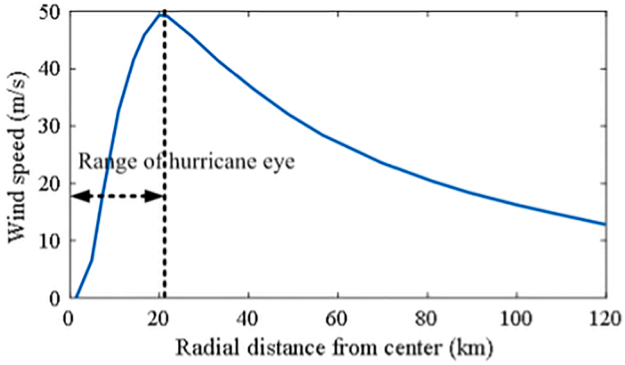

Fig. 1. Radial wind speed profile of a hurricane eye: An example.

2.3. Routing of repair crew

After natural disasters, the DSO will dispatch repair crews to replace damaged distribution poles and to fix faulted lines. After a natural disaster, it is necessary to determine the optimal repair sequence in order to minimize the operating cost. An example of repair crew routing is shown in Fig. 2. In this event, there are three faults and one available repair crew. The repair sequence is determined as: The repair crew travels from the depot to Fault #2, Fault #3, and Fault #1 in turn to repair the damaged components. The total time consumption for a repair action ($\overline{T}_{ij}^{rep}$) consists of two parts, given in.

$$\overline{T}_{ij}^{rep} = T_{ij,p}^{tr} + T_{ij}^{rep}, \quad \forall (i,\ j) \in \Omega_{B,Fa} \tag{1}$$

where $T_{ij,p}^{tr}$ is the travel time from a position p to the faulted line (i, j), and p can be the repair crew depot (central crew stations) or the last faulted line being repaired; T_{ij}^{rep} is the forecast time consumption to repair the line (i, j). The detailed forecast method was introduced in [29]. In the urban area, a distribution system is usually geographically within 10 km. Even if considering a low traveling speed of trucks that caring the repair crew and goods (20 km/hour), the traveling time between any two locations within the distribution system ($T_{ij,p}^{tr}$) is below 0.5 h. Since the repair time is usually 3–8 h [29,30], there is$T_{ij,p}^{tr} \leqslant T_{ij}^{rep}$. Therefore, $\overline{T}_{ij}^{rep}$ can be approximated by a constant value without considering the traveling path, as given by.

$$\overline{T}_{ij}^{rep} = \lceil T^{tr} + T_{ij}^{rep} \rceil, \quad \forall (i,\ j) \in \Omega_{B,Fa} \tag{2}$$

The rounding up sign $\lceil\rceil$ provides the repair action with a time margin and eliminates the forecast error of$\overline{T}_{ij}^{rep}$. For example, if $T^{tr} + T_{ij}^{rep}$ is forecast to be 5.3 h, then the DSO assumes it takes $\overline{T}_{ij}^{rep} = 6$ h to repair the line (i, j). The repair crew can finish the work on time even if the repair action has an error of 0.7 h.

Based on the above analysis, the following assumptions are made in order to simplify the optimization algorithm.

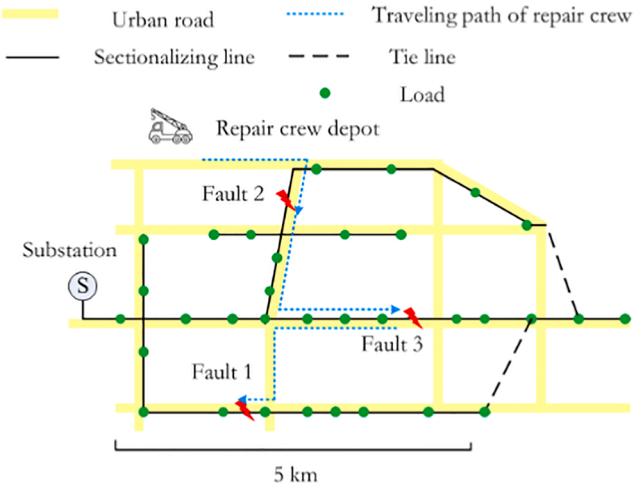

Fig. 2. Illustration of repair crew path.

- The working efficiency of different repair crews is the same. In other words, different repair crews take the same time $\overline{T}_{ij}^{rep}$ to repair the same faulted line (i, j) [15]. The DSO is able to locate the faulted lines and to estimate $\overline{T}_{ij}^{rep}$ [17].
- Damage to the road network does not have an obvious impact on $T_{ij,p}^{tr}$. This is because the repair crew truck has multiple routing options to reach the same destination via the road network [31].

3. Operational planning of repair and restoration

The DSRR is a co-optimization of 1) repair crew scheduling, 2) dynamic network reconfiguration that is coupled with line repair status, and 3) DER scheduling and load shedding. The feature of those three groups of decision variables can be summarized as follows.

- *Decision variable of repair scheduling*: The repairing of a faulted line takes multiple hours or time steps. Thus, the scheduling of repair crews involves inter-time-step constraints. Once the scheduling of crews is executed, it is not feasible to re-dispatch it when the line repair is ongoing.
- *Decision variable of network reconfiguration*: The network reconfiguration is implemented by the change of switching states. Since there is an upper limit of switching state change (given by Eq. (17)), it is not feasible to re-dispatch the network reconfiguration at each time step.
- *Decision variable of power output/demand*: The fuel-based DG is started to serve the local load. Meanwhile, part of load is curtailed due to the limited capacity of DG. These two decision variables are independent among different time steps.

Based on the features of post-disaster operation of distribution system, this paper proposes a two-stage DSRR strategy to minimize the cost of DG operation and load shedding. As shown in Fig. 3, the first stage determines the repair scheduling, dynamic reconfiguration, and DG output/load shedding based on the forecast of load demand and PV power output. However, the forecast error may cause a violation of the load reduction limit and line thermal limit when the decision variable is executed at later time steps. Therefore, the second stage re-dispatch is proposed to avoid this violation. At each time step, the decision maker executes the repair scheduling and network reconfiguration decisions made in the first stage, while adjusts the DG and load shedding decision based on the latest PV output and load demand.

3.1. Co-Optimization of Repair, reconfiguration and DER

The first stage of the proposed DSRR strategy performs multi-time-interval scheduling in order to minimize the expected operating cost.

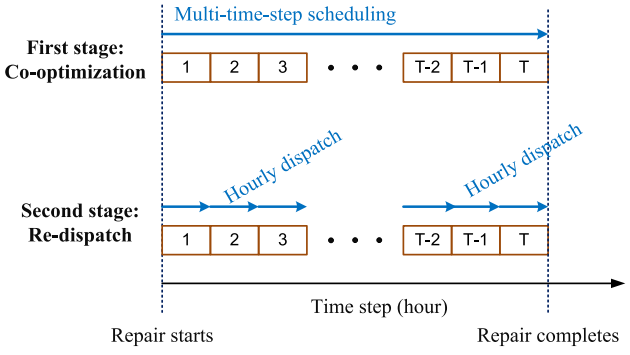

Fig. 3. Time step of two-stage DSRR.

3.1.1. Objective function

The objective function is formulated as Eq. (3), which consists of the operating cost of fuel-based DGs and the cost of unserved loads. Δt is the scheduling time interval.

$$min. \sum_{t\in\Omega_T}\Delta t\left(\sum_{j\in\Omega_{N,G}} c^G \widehat{P}_{j,t}^G + \sum_{j\in\Omega_N} c^L \Delta\widehat{P}_{j,t}^L\right) \tag{3}$$

During the period Ω_T, the network topology may change at any hour. However, the total number of switch changes in one line can be restricted. Indeed, supplying as much electricity to loads as possible under extreme weather conditions is more important than reducing the operating expense of DGs. However, since the per-kWh generation cost is usually lower than the load shedding cost in (3), the operating cost minimization is equivalent to the load shedding minimization, which is a measure of resilience against extreme weather. This is the justification for including both the DG term and the load term in (3).

3.1.2. Repair crew scheduling constraints

In this paper, we consider a case wherein multiple crews work simultaneously and independently on the repair of separate lines. The constraints for optimal repair crew dispatching are given by (4)–(9). Since equations (4)–(34) are all time-dependent, the expression $\forall t \in \Omega_T$ behind each equation is omitted for simplicity.

$$\mu_{ij,t} = 0, \quad \forall(i, j) \in \Omega_{B,Fa}, \quad t \leqslant \overline{T}_{ij}^{rep} \tag{4}$$

$$y_{ij,t} = \sum_{\tau=1}^{t} \mu_{ij,\tau}, \quad \forall(i, j) \in \Omega_{B,Fa} \tag{5}$$

$$z_{ij,t} \leqslant y_{ij,t}, \quad \forall(i, j) \in \Omega_{B,Fa} \tag{6}$$

$$\sum_{t=1}^{|\Omega_T|} \nu_{ij,t} = \overline{T}_{ij}^{rep}, \quad \forall(i, j) \in \Omega_{B,Fa} \tag{7}$$

$$-M_1\left(1-\mu_{ij,t}\right) \leqslant \sum_{\tau=t-T_{ij}^{rep}}^{t-1} \nu_{ij,\tau} - \overline{T}_{ij}^{rep} \leqslant 0, \quad \forall(i, j) \in \Omega_{B,Fa} \tag{8}$$

$$\sum_{\forall ij} \nu_{ij,t} \leqslant N^{rep}, \quad \forall(i, j) \in \Omega_{B,Fa} \tag{9}$$

Constraint (4) initializes the status of faulted lines. Even if the faulted line (i, j) is assigned to be repaired first, the line stays open during the beginning $\overline{T}_{ij}^{rep}$ hours. Constraint (5) indicates that the faulted line becomes available after it is repaired and remains available in all subsequent hours. Constraint (6) connects the line switch availability and the distribution system reconfiguration. If the faulted line (i, j) is normal ($y_{ij,t} = 1$), then the line switching state is a free binary variable (either on or off). Otherwise, the line will be open if it is not repaired ($y_{ij,t} = 0$). Constraint (7) means that during the DSRR period Ω_T, the total number of hours spent on the faulted line (i, j) equals the predicted time $\overline{T}_{ij}^{rep}$. Constraint (8) indicates that the repair crew works on the faulted line (i, j) for $\overline{T}_{ij}^{rep}$ consecutive hours before the line is repaired. The correlation between $\nu_{ij,t}$ and $\mu_{ij,t}$ is given by a "big M" inequality constraint, where M_1 is a sufficiently large number. If the faulted line is repaired at hour t, then $\mu_{ij,t} = 1$ and $\sum_{\tau=t-T_{ij}^{rep}}^{t-1} \nu_{ij,\tau} - \overline{T}_{ij}^{rep} = 0$. Therefore, the only solution for this equation is $\nu_{ij,\tau} = 1$ ($\tau = t - \overline{T}_{ij}^{rep}, t - \overline{T}_{ij}^{rep} + 1, \ldots t - 1$). Otherwise, $\sum_{\tau=t-T_{ij}^{rep}}^{t-1} \nu_{ij,\tau} - \overline{T}_{ij}^{rep}$ is unbounded. Constraint (9) means that during the restoration period, a maximum of N^{rep} repairing crews work on the faulted lines.

In order to better illustrate the constraints (4)–(9), Fig. 4 shows a simple example of the evolution of binary variables $\nu_{ij,t}$, $\mu_{ij,t}$, and $y_{ij,t}$. Three faulted lines (Line #1, #2, and #3) needs to be repaired by two available repair crews (A and B). The $\overline{T}_{ij}^{rep}$ value of three lines is forecast

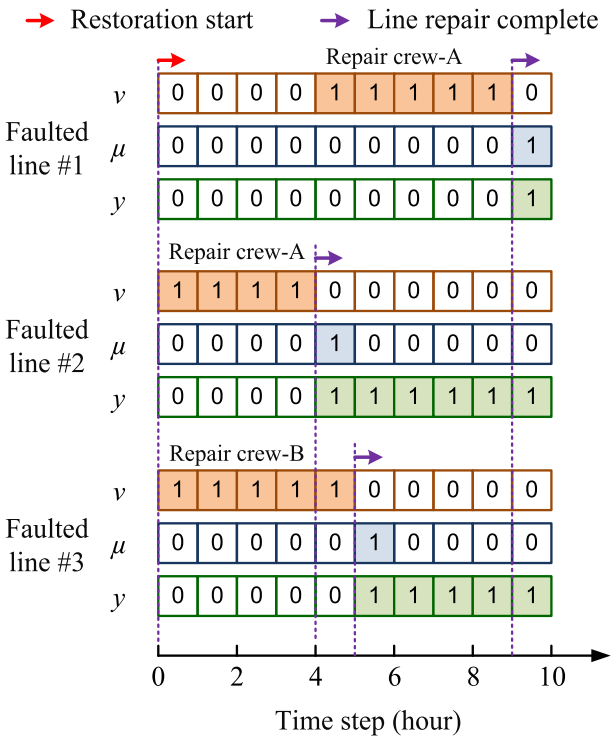

Fig. 4. Illustration of repair crew scheduling status.

to be 5 h, 4 h, and 5 h, respectively. A feasible solution for this scheduling problem is as follows:

- At the beginning of the 1st hour, the restoration process starts. Sending the repair crew-A to the faulted line #2 and crew-B to faulted line #3.
- At the beginning of the 5th hour, crew-A successfully repairs line #2. Then, sending crew-A to faulted line #1.
- At the beginning of the 6th hour, crew-B successfully repairs line #3. Then, crew-B doesn't need to work on other lines.
- At the beginning of the 10th hour, all faulted lines are repaired and the whole restoration is completed.

3.1.3. Network topology constraints

Normally, a connected graph without cycles is defined as a radial graph [33]. A simple example is shown in Fig. 5. The single commodity flow (SCF) is an effective method to model the radial-topology constraints as a set of linear equations [7]. In this study, the SCF method is adopted. We introduce a lossless fictitious network that has the same topology and the same group of switching status variables z^{s}_{ij} as the original electric network. In the fictitious network, each non-source bus is assumed to have the unity load demand 1.0, as shown in Fig. 5. The radial-topology constraints are given by (10)–(14).

$$\sum_{ij} z_{ij,t} \leqslant N-1, \quad \forall (i,j) \in \Omega_B \tag{10}$$

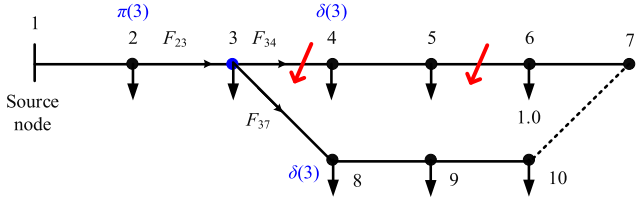

Fig. 5. Example of a radial network.

$$\sum_{k\in\delta(j)} F_{jk,t} - \sum_{i\in\pi(j)} F_{ij,t} = -1, \quad \forall j \in \Omega_N, j \neq 1 \tag{11}$$

$$-M_2 z_{ij,t} \leqslant F_{ij,t} \leqslant M_2 z_{ij,t}, \quad \forall (i,j) \in \Omega_B \tag{12}$$

$$\sum_{k\in\delta(j)} F_{jk,t} \leqslant N-1, \quad j=1, \forall (j,k) \in \Omega_B \tag{13}$$

$$z_{ij,t} = 1, \quad \forall (i,j) \in \Omega_{B,NS} \backslash \Omega_{B,Fa} \tag{14}$$

Constraint (10) ensures that the number of closed lines does not exceed the number of non-source buses [5]. Constraint (11) represents the line flow balance of a bus. If a bus belongs to an island, it is de-energized and does not serve the load. Constraint (12) is the line flow constraint, where M_2 is a sufficiently large number. Constraint (13) means that if the network is a connected graph, the line flow through the source bus does not exceed the number of non-source buses. Constraint (14) indicates that a line without an RCS will stay closed if not tripped. Fixing these binary variables by (14) will improve the computational efficiency.

The maximal switching time of each RCS is restricted by (15)–(17): $s_{ij,t}=0$ only if $z^{ij,t-1}=z_{ij,t}=0$ or $z^{ij,t-1}=z_{ij,t}=1$, otherwise $s^{ij,t}=1$. N^{sw} can be specified by the decision maker considering the wear and tear of RCSs.

$$s_{ij,t} \geqslant z_{ij,t-1} - z_{ij,t}, \quad \forall (i,j) \in \Omega_B \backslash \Omega_{B,NS}, \ t \geqslant 2 \tag{15}$$

$$s_{ij,t} \geqslant z_{ij,t} - z_{ij,t-1}, \quad \forall (i,j) \in \Omega_B \backslash \Omega_{B,NS}, \ t \geqslant 2 \tag{16}$$

$$\sum_{t=2}^{|\Omega_T|} s_{ij,t} \leqslant N^{sw}, \quad (i,j) \in \Omega_B \backslash \Omega_{B,NS} \tag{17}$$

3.1.4. System operating constraints

The DSRR strategy should satisfy the device operating constraints and power flow constraints, given by (18)–(34).

$$0 \leqslant \widehat{P}^{G}_{j,t} \leqslant P^{Gmax}_{j}, \quad \forall j \in \Omega_{N,G} \tag{18}$$

$$0 \leqslant \Delta\widehat{P}^{L}_{j,t} \leqslant \widehat{P}^{L}_{j,t}, \quad \forall j \in \Omega_N \tag{19}$$

$$\widehat{P}^{L}_{j,t} = K_t \cdot P^{L}_{j}, \quad \forall j \in \Omega_N \tag{20}$$

$$\beta_j = \frac{\sqrt{1-PF_j^2}}{PF_j}, \quad \forall j \in \Omega_N \tag{21}$$

$$\Delta\widehat{Q}^{L}_{j,t} = \beta_j \Delta\widehat{P}^{L}_{j,t}, \quad \forall j \in \Omega_N \tag{22}$$

$$E^{B}_{j,1} = E^{B}_{j,start}, \quad \forall j \in \Omega_{N,E} \tag{23}$$

$$-\overline{P}^{Bdch}_{i} \leqslant P^{Bdch}_{j,t} \leqslant \overline{P}^{Bdch}_{i}, \quad \forall j \in \Omega_{N,E} \tag{24}$$

$$E^{B}_{j,t+1} = E^{B}_{j,t} - P^{Bdch}_{j,t}\Delta t, \quad \forall j \in \Omega_{N,E} \tag{25}$$

$$SoC_{min}\overline{E}^{B}_{j} \leqslant E^{B}_{j,t} \leqslant SoC_{max}\overline{E}^{B}_{j}, \quad \forall j \in \Omega_{N,E} \tag{26}$$

$$\sum_{k\in\delta(j)} P_{jk,t} - \sum_{i\in\pi(j)} P_{ij,t} = \widehat{P}^{G}_{j,t} + \widehat{P}^{PV}_{j,t} + P^{Bdch}_{j,t} + 0 - \left(\widehat{P}^{L}_{j,t} - \Delta\widehat{P}^{L}_{j,t}\right), \quad \forall j \in \Omega_N, j \neq 1, \forall (i,j) \in \Omega_B, \forall (j,k) \in \Omega_B \tag{27}$$

$$\sum_{k\in\delta(j)} Q_{jk,t} - \sum_{i\in\pi(j)} Q_{ij,t} = 0 + 0 + 0 + Q^{C}_{j,t} - \left(\widehat{Q}^{L}_{j,t} - \Delta\widehat{Q}^{L}_{j,t}\right), \quad \forall j \in \Omega_N, j \neq 1, \forall (i,j) \in \Omega_B, \forall (j,k) \in \Omega_B \tag{28}$$

$$Q^{C}_{j,t} = Q^{Crt}_{j}\left(V_{j,t}\right)^2 \approx Q^{Crt}_{j}\left(2V_{j,t}-1\right), \quad \forall j \in \Omega_{N,C} \tag{29}$$

$$-M_3\left(1-z_{ij,t}\right)\leqslant V_{i,t}-V_{j,t}-\left(R_{ij}P_{ij,t}+X_{ij}Q_{ij,t}\right)\leqslant M_3\left(1-z_{ij,t}\right),\quad \forall(i,\ j)\in\Omega_B \tag{30}$$

$$-S_{ij}^{max}z_{ij,t}\leqslant P_{ij,t}\leqslant S_{ij}^{max}z_{ij,t},\quad \forall(i,\ j)\in\Omega_B \tag{31}$$

$$-0.5S_{ij}^{max}z_{ij,t}\leqslant Q_{ij,t}\leqslant 0.5S_{ij}^{max}z_{ij,t},\quad \forall(i,\ j)\in\Omega_B \tag{32}$$

$$V^{min}\leqslant V_{j,t}\leqslant V^{max},\quad \forall j\in\Omega_N,\ j\neq 1 \tag{33}$$

$$V_{1,t}=V_{sub} \tag{34}$$

Constraint (18) represents the power output limit of fuel-based DG. Constraint (19) indicates that the amount of load shedding cannot exceed the existing load. Generally, thermostatic loads (e.g., air conditioners) are of high priority to be turned off [32]. Constraint (20) computes the load profile of each bus, where K_t is the normalized load profile. Based on the assumption that the power factors of both the critical load (CL) and interruptible load (IL) are constant at all times, the ratio between the reactive and real powers of a load is expressed as (21). Hence, the reactive power variables can be replaced with active power variables, given by (22). Constraint (23) initializes the battery energy. All BESSs will be pre-charged to 100% state-of-charge (SOC) before the hurricane reaches the target distribution system. Since the latest Lithium-ion battery has high round-trip efficiency (92–96%) [34,35], this study assumes 100% efficiency of BESSs in order to simplify the optimization model. Therefore, constraint (24) expresses the net discharging limit, in which the charging power has been converted to negative discharging power. Constraint (25) expresses the BESS energy change at each hour. Constraint (26) restricts the SOC limit of a BESS. The real and reactive power injections to bus j are given by (27)–(28). Note: the reactive power output of a fuel-based DG, PV system and BESS are denoted as zeros. Also, the real power output of a capacitor is denoted as zero. As a result, constraints (27)–(28) have similar forms. The reactive power of a shunt capacitor (SC) is linearized as (29) due to the tight range of the voltage. According to the linearized DistFlow method, constraint (30) restricts the line voltage drop. If $z^{ij,t}=1$, the inequality constraint is reduced to an equality constraint, while if $z^{ij,t}=0$, then $V^{i,t}-V^{j,t}$ is unbounded. Constraints (31)–(32) ensure that the power flow through line (i, j) is zero if it is open. If the line (i, j) is closed, the reactive power limit is assumed to be half of the thermal limit of the line [10]. The voltage limits are given by (33). Bus 1 is the slack (substation) bus, given by (34). Above all, the co-optimization problem is formulated as a mixed-integer linear programming (MILP).

3.2. Hourly Re-dispatch of DER

At the t-th hour ($t \geq 2$) of the DSRR process, the objective function is to minimize the operating cost.

$$min.\ \left(\sum_{j\in\Omega_{N,G}}c^G P_{j,t}^G+\sum_{j\in\Omega_N}c^L\Delta P_{j,t}^L\right),\quad \forall t\in\Omega_T \tag{35}$$

The network reconfiguration is executed by the DSO, as given by (36). The symbol (.)* indicates the solution obtained by the first-stage optimization. Since the network topology is determined, the inequality constraint (30) is reduced to an equality constraint (37).

$$z_{ij,t}=z_{ij,t}^{*},\quad \forall(i,\ j)\in\Omega_B \tag{36}$$

$$R_{ij}P_{ij,t}+X_{ij}Q_{ij,t}=V_{i,t}-V_{j,t},\quad \forall(i,\ j)\in\Omega_B,\ z_{ij,t}=1 \tag{37}$$

The practical load demand may deviate from the forecast value. The forecast errors of load and PV output are modeled as random multipliers $\chi_{j,t}^L$, $\chi_{j,t}^{PV}$ that follow normal distributions $N(1, \sigma_L^2)$ and $N(1, \sigma_{PV}^2)$, as enforced by (38) and (39), respectively. Thus, the real power reduction is limited by (41). The corresponding reactive power reduction is given by (42). Since the net discharging power of a BESS is time-dependent, the BESS power output is the same as the first stage (43).

$$P_{j,t}^L=\chi_{j,t}^L\cdot M_t\cdot P_j^L,\quad \forall j\in\Omega_N,\ t\in\Omega_T \tag{38}$$

$$P_{j,t}^{PV}=\chi_{j,t}^{PV}\cdot\widehat{P}_j^{PV},\quad \forall j\in\Omega_N,\ t\in\Omega_T \tag{39}$$

$$0\leqslant P_{j,t}^G\leqslant P_j^{Gmax},\quad \forall j\in\Omega_{N,G} \tag{40}$$

$$0\leqslant\Delta P_{j,t}^L\leqslant P_{j,t}^L,\quad \forall j\in\Omega_N \tag{41}$$

$$\Delta Q_{j,t}^L=\beta_j\Delta P_{j,t}^L,\quad \forall j\in\Omega_N,\ t\in\Omega_T \tag{42}$$

$$P_{j,t}^{Bdch}=P_{j,t}^{Bdch*},\quad \forall j\in\Omega_N,\ t\in\Omega_T \tag{43}$$

Then, the constraints (19), (27), and (28) are rewritten as (41), (44), and (45), respectively.

$$\sum_{k\in\delta(j)}P_{jk,t}-\sum_{i\in\pi(j)}P_{ij,t}=P_{j,t}^G+P_{j,t}^{PV}+P_{j,t}^{Bdch}+0-\left(P_{j,t}^L-\Delta P_{j,t}^L\right),\forall j\in\Omega_N,j\neq 1 \tag{44}$$

$$\sum_{k\in\delta(j)}Q_{jk,t}-\sum_{i\in\pi(j)}Q_{ij,t}=0+0\ +\ 0+Q_{j,t}^C-\left(Q_{j,t}^L-\Delta Q_{j,t}^L\right),\forall j\in\Omega_N,j\neq 1 \tag{45}$$

In the second stage, the decision variables are all continuous variables, and the optimization is in the form of linear programming.

3.3. Summary of the two-stage DSRR

Based on the analysis in Sections 3.1 and 3.2, the two-stage DSRR strategy is summarized in Fig. 6. After the disaster is over, the DSO locates the faulted lines and conducts the first stage DSRR, which is an $|\Omega_T|$-hour-ahead co-optimization of repair crews, reconfiguration, and DER dispatch. The first stage is a mix-integer linear programming (MILP), including $|\Omega^T|\times(3\times|\Omega^{B,Fa}|+2\times|\Omega^B|)$ binary variables and $|\Omega^T|\times(3\times|\Omega^B|+5\times|\Omega^N|)$ continuous variables. Generally, the number of binary variables will be less than $|\Omega^T|\times(3\times|\Omega^{B,Fa}|+2\times|\Omega^B|)$ because

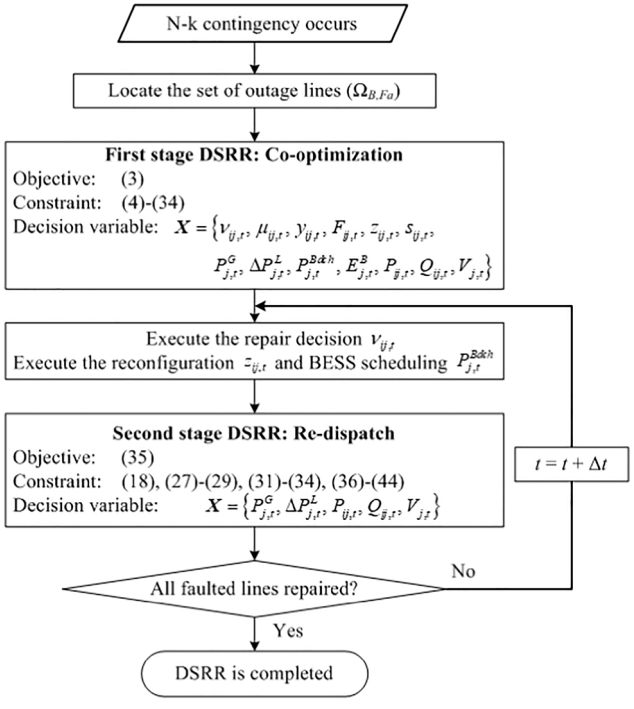

Fig. 6. Flowchart of two-stage DSRR.

not all lines are equipped with RCSs. At each hour, the decisions of repair crew dispatch and dynamic network reconfiguration are executed. The second-stage re-dispatch is done based on the deterministic binary variables (obtained in the first stage) and the latest load demand$P^L_{j,t}$. This stage only involves continuous variables. The re-dispatch continues until all faulted lines are repaired. The programming of both stages can be directly solved by commercial solvers.

4. Case study

This section presents comprehensive case studies on the modified IEEE 33-bus and IEEE 123-bus test systems. The computational tasks are performed on a personal laptop computer with an Intel Core i7 Processor (3.00 GHz) and 16-GB RAM, and the code is implemented via the Matlab-based IBM ILOG CPLEX Optimization Studio V12.8.0.

4.1. IEEE 33-bus system

The modified IEEE 33-bus system is shown in Fig. 7. The system parameters are given in Table 1. Loads are classified into CLs and ILs. Examples of CLs are industrial, government and hospital loads, while ILs are generally residential loads. CLs and ILs can be turned off for different payments, reflecting the importance or reliability requirement of different types of users [36]. The load profiles are diverse. To simplify the study, this paper adpots one type of CL and IL profiles, respectively (shown in Fig. 8). The CLs at different buses adopt the same base CL profile. Similarly, the ILs at different buses adopt the same base residential load profile. In this study, the random multipliers $\chi^L_{j,t} \sim N(1, 0.10^2)$ and $\chi^{PV}_{j,t} \sim N(1, 0.10^2)$ are applied to the base load profile to model the load/PV forecast error.

The parameters of the two scenarios are shown in Table 2. The DSRR starts at the hour when the hurricane leaves the distribution system. In order to demonstrate the importance of optimal repair dispatch, we compare the results of two methods in each scenario:

- Method 1 is the proposed two-stage DSRR with optimal repair sequence, reconfiguration and DER scheduling.
- Method 2 is the reduced version of DSRR, in which the repair sequence is determined in an empirical manner. In other word, the variables $\nu_{ij,t}$, $y^{ij,t}$ and $\mu^{ij,t}$ are specified while the network reconfiguration and DER scheduling are solved in the same way as Method 1.

The first scenario considers three faulted lines and one repair crew. The time horizon for DSRR is determined as: $|\Omega_T| = 5 + 4 + 4 + 1 = 14$ h. The repair scheduling of Method 1 (optimal repair sequence) and

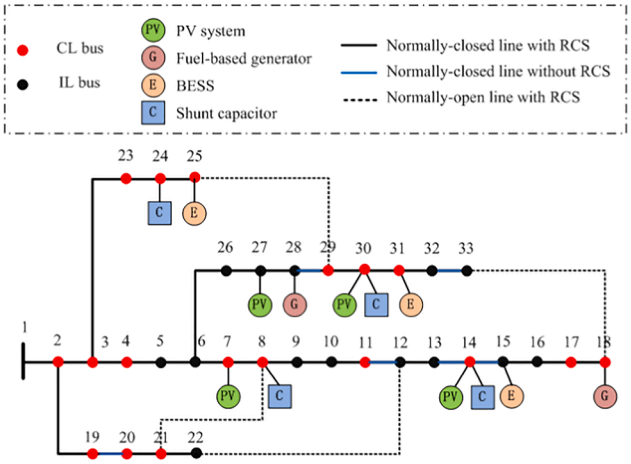

Fig. 7. IEEE 33-bus system with DERs.

Table 1
Parameters of IEEE 33-bus system.

Class	Parameter	Value
System components	Load	3.715 MW + j 2.300 Mvar
	Fuel-based generator	Two devices, 0.40 MW capacity
	PV systems	Four devices, 0.36 MW capacity
	Energy storage	Three devices, 0.45 MW/1.4 MWh capacity, 100% initial SOC
	Shunt capacitors	Four devices, 1.1 Mvar capacity
Cost	c^G	\$0.25 k/MWh
	c^L_j	\$1.2 k/MWh (CL) \$0.5 k/MWh (IL)
System voltage	V_{min}	0.95p.u.
	V_{max}	1.05p.u.
	V_{sub}	0.99p.u.

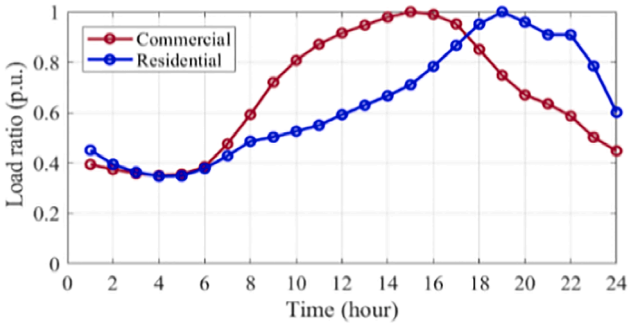

Fig. 8. Commercial and residential load profiles.

Table 2
Parameters of scenarios.

Scenario	Starting time of DSRR	Faulted lines and predicted repair time	N^{rep}	N_{sw}
1	10:00	Line (4, 5), (23, 24), (27, 28) $\overline{T}^{rep}_{4,5} = 5, \overline{T}^{rep}_{23,24} = 4, \overline{T}^{rep}_{27,28} = 4$	1	3
2	11:00	Line (4, 5), (8, 9), (3, 23), (27, 28) $\overline{T}^{rep}_{4,5} = 5, \overline{T}^{rep}_{8,9} = 3, \overline{T}^{rep}_{3,23} = 4, \overline{T}^{rep}_{27,28} = 5$	2	3

Method 2 (empirical repair sequence) is visualized in Fig. 9. During the DSRR period, the DSO may change the switching states of lines at each hour but ensures that the total number of switching changes is within the N^{sw} limit. The network reconfiguration at four representative hours is shown in Fig. 10. Before the faulted lines are repaired, islanded parts of the system are picked up by adjacent feeders through tie lines. The reason for repairing Line (23, 24) first can be intuitively explained: 1) $S^{max}_{23,24}$ is relatively large; 2) connecting Line (23, 24) can restore a large amount of CL at Bus # 28-33 during the subsequent hours by reconfiguration (see Fig. 10 (b)). The result also indicates that the optimal repair sequence is coupled with dynamic topology reconfiguration.

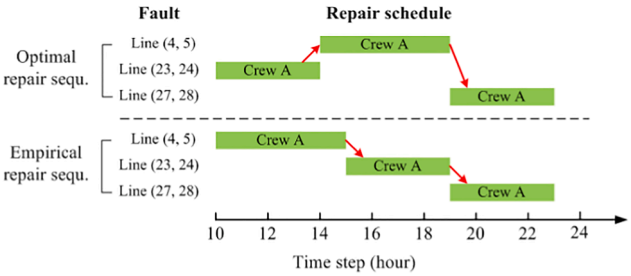

Fig. 9. Repair sequence of Method 1 and 2.

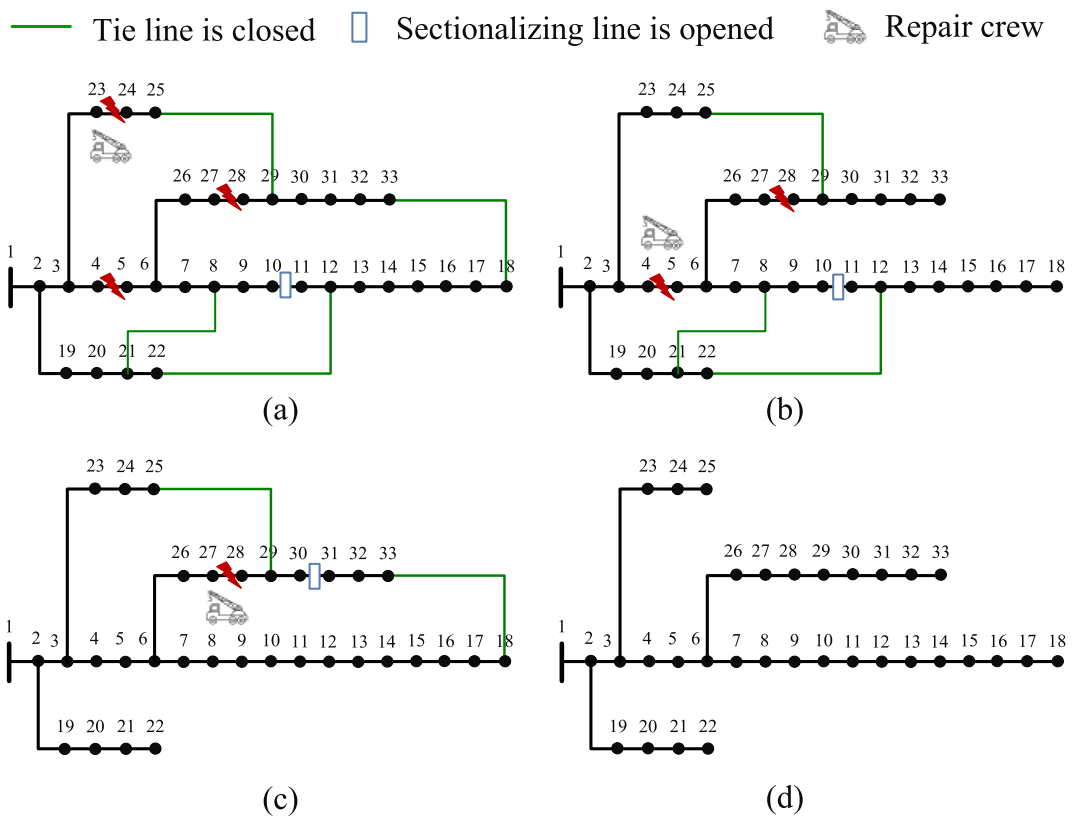

Fig. 10. Dynamic network reconfiguration with optimal repair sequence: (a) At the 10th hour; (b) At the 15th hour; (c) At the 19th hour; (d) At the 23rd hour.

The second-stage re-dispatch modifies the optimal DG output and load shedding. In Method 1, the repair progress of faulted lines and the total amount of served load are presented in Fig. 11. The "Normal" case means that there is no fault in the system. During the 10th − 13th hours, three upstream lines are faulted. The restored load is restricted by the line thermal limits (of Line (2, 19)) and DER capacity. During the 14th18th hours, Line (23, 24) is repaired and reclosed. Therefore, a larger amount of load can be served by the substation. Although ILs are still unserved, almost all CLs are restored. During the 19th − 22nd hour, Line (4, 5) is also repaired. Thus, all loads can be served by network reconfiguration only. The total cost during DSRR is $6946. The computational time for the two-stage optimization is 6.9 s.

In comparison, Method 2 (with empirical repair sequence) shows a lower restored CL and IL with the same resources and fault scenario. The total cost is $7810, which is 12.4% higher than that of Method 1. The main reason can be explained from Fig. 9 and Fig. 11: 1) it takes one more hour to repair Line (4, 5) than to repair Line (23, 24); 2) both lines serve a large amount of load. Then, Method 1 makes a larger amount of load be picked up when the first faulted line is repaired.

In the second scenario, there are four faulted lines and two repair crews. The DSRR horizon is determined as: $|\Omega_T| = 5 + 5 + 1 = 11$ h. The repair sequence of Method 1 and 2 is visualized in Fig. 12. The network reconfiguration at four representative hours is shown in Fig. 13. The network topology keeps changing at each hour, but the switching state of each line changes no more than N^{sw} times. The repair progress of faulted lines and the total amount of restored load are presented in Fig. 14. At $t = 15$th hour, Line (3, 23) is repaired and reclosed. Therefore, a larger amount of CL can be served by the substation. When the second

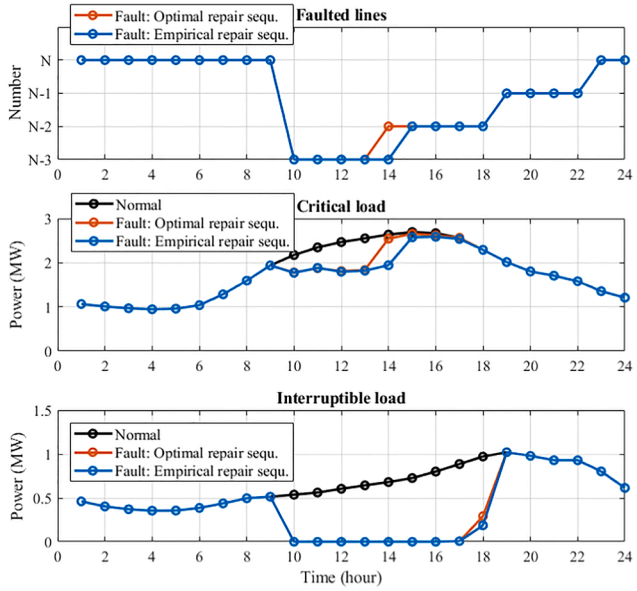

Fig. 11. Progress of line repair and load restoration.

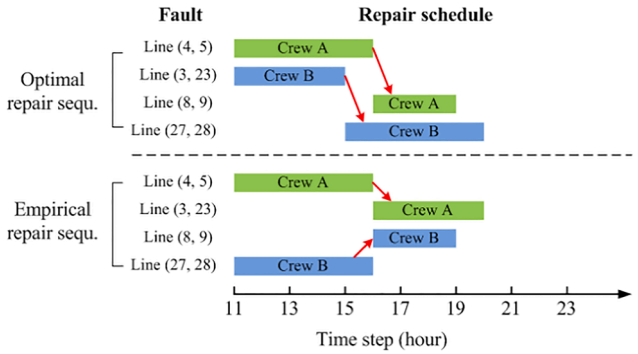

Fig. 12. Repair sequence of Method 1 and 2.

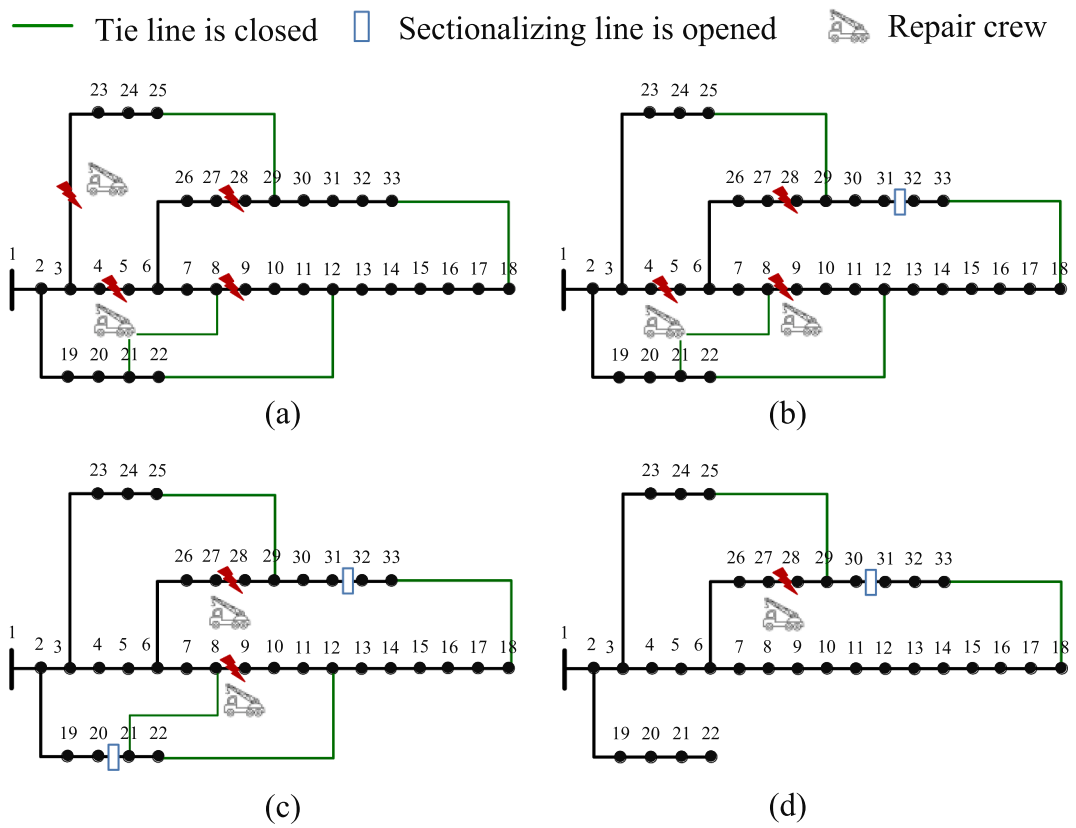

Fig. 13. Dynamic network reconfiguration with optimal repair sequence: (a) At the 10th hour; (b) At the 15th hour; (c) At the 17th hour; (d) At the 19th hour.

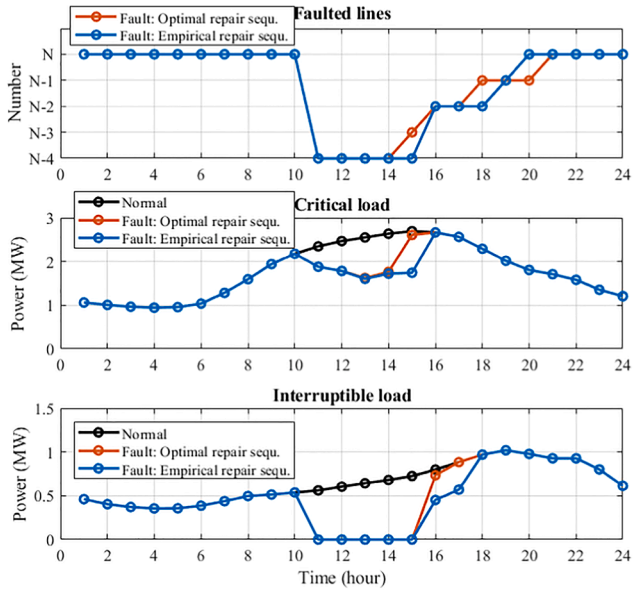

Fig. 14. Progress of line repair and load restoration.

faulted line is repaired at $t = 16$th hour, a larger portion of CLs and ILs are restored by network reconfiguration. The total operating cost of Method 1 is \$6082.

The computation time is 8.8 s.

By contrast, the total cost of Method 2 is \$7404 for the same resources and fault scenario as Method 1. Similarly, the main reason for higher cost is that the crews are arranged to repair the time-consuming lines (Line (4, 5) and (27, 28)). Then, the 15th hour suffers a higher load shedding than Case 2.

4.2. IEEE 123 bus system

Fig. 15 shows the modified single-phase IEEE 123-bus system. The five normally-open tie lines are 29–48, 39–66, 54–94, and 115–116. Among the 121 lines, 22 normally-closed lines and 4 normally-open lines are installed with automatic switches. The parameters of system component, cost and system are listed in Table 3. The same set of CL and

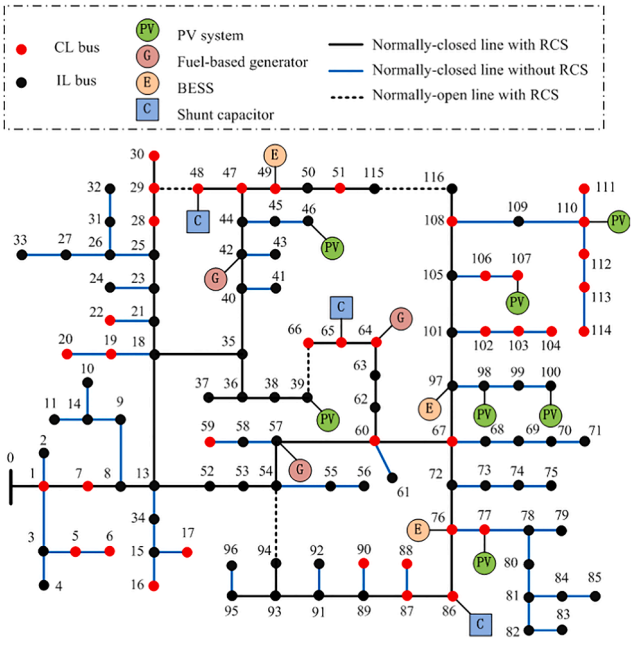

Fig. 15. IEEE 123-bus system with DERs.

Table 3
Parameters of IEEE 123-bus system.

Class	Parameter	Value
System components	Load	7.060 MW + j 3.880 Mvar
	Fuel-based generator	Three devices, 0.72 MW capacity
	PV systems	Seven devices, 0.50 MW capacity
	Energy storage	Three devices, 0.60 MW/2.4 MWh capacity, 100% initial SOC
	Shunt capacitors	Three devices, 0.84 Mvar capacity
Cost	c^G	\$0.25 k/MWh
	c_j^L	\$1.2 k/MWh (CL) \$0.5 k/MWh (IL)
System voltage	V_{min}	0.95p.u.
	V_{max}	1.05p.u.
	V_{sub}	0.99p.u.

IL profiles are adopted, as shown in Fig. 8. The parameters of a fault scenario are shown in Table 4.

In this system, there are five faulted lines and two repair crews. The DSRR horizon is determined as: $|\Omega_T| = 13$ h. Fig. 16 illustrate the repair sequence of Method 1 and 2. The optimization finds that the upstream lines (13, 52) and (40, 42) should be repaired first. Crew 1 and Crew 2 travel to Line (87, 89) and Line (67, 97) after finishing the repair of the first two lines, respectively.

The second-stage re-dispatch obtains the hourly DG output and load shedding. Fig. 17 presents the restoration progress of faulted lines and total restored CL/IL. At the 15th and 16th hour, two upstream lines (13, 52) and (40, 42) are repaired, respectively. Almost all loads are restored during the subsequent hours. The total operating cost is \$7522. The computation time is 61.2 s. Furthermore, the total cost of Method 2 is \$9180. The result verifies that the optimal repair sequence can minimize the load shedding cost during the DSRR period. Similarly, the high cost is also caused by the non-optimal repair sequence: the Crew B is sent to first repair the time-consuming line (67, 97). Also, Line (67, 97) provides less capacity than Line (40, 42).

The studies of IEEE 33-bus and 123-bus systems indicate that the operational plannings of repair sequence and network reconfiguration are closely coupled. Intuitively, the lines which locates at the upstream feeder and take shorter repairing time should be selected to be repaired first (named as "upstream and shorter time" for simplicity). However, it is hard to empirically determine the repair sequence of such lines with "upstream and longer time" or "downstream and shorter time". Therefore, the proposed optimal DSRR determine the best repair sequence and the corresponding network reconfiguration. The comparison between Method 1 and 2 also serves as a sensitivity study to demonstrate the effect of optimal repair sequence on reducing the cost. The two-stage DSRR guarantees the optimal repair sequence that is coupled with dynamic network reconfiguration. As a compensation of the first-stage, the second-stage re-dispatch provides the optimal DG and load dispatch according to the latest load/PV profile.

5. Conclusion

The DSRR is a cooperative dispatch of multiple distribution system resources, including repair crews, normal-open tie lines and DERs. It conducts the repair and restoration simultaneously to minimize the unserved load. This paper develops a DSRR strategy to enhance the resilience of distribution systems against N-k contingencies with the consideration of load demand uncertainty. The main contributions of this paper are two-fold.

- In the first stage, the co-optimization model solves for the optimal repair sequence and dynamic network reconfiguration simultaneously, together with the DER dispatch. The correlation between the repair crew allocation and the line switching states are modeled as a set of simple linear constraints. The maximal number of switching actions can be specified in order to prevent the wear and tear of RCSs. Once the faulted line is repaired, its switching state becomes a free binary variable at the subsequent hours. As a result, the repaired lines can be fully utilized to restore more loads. The method is more applicable to geographically-compact distribution systems.
- Based on the optimal repair scheduling and network reconfiguration, a re-dispatch of DER scheduling based on the latest input parameters is proposed to overcome the prediction error of the load profile. Since the binary variables have been determined in the first stage, the re-dispatch is in the form of linear programming and requires low computational workload.

In light of the rapid development of mobile power sources, future

Table 4
Parameters of scenarios.

Scenario	Starting time of DSRR	Faulted lines and predicted repair time	N^{rep}	N_{sw}
1	11:00	Line (13, 52), (40, 42), (67, 97), (80, 81), (87, 89) $\overline{T}^{rep}_{13,52} = 5, \overline{T}^{rep}_{40,42} = 4, \overline{T}^{rep}_{67,97} = 6, \overline{T}^{rep}_{80,81} = 3, \overline{T}^{rep}_{87,89} = 3$	2	4

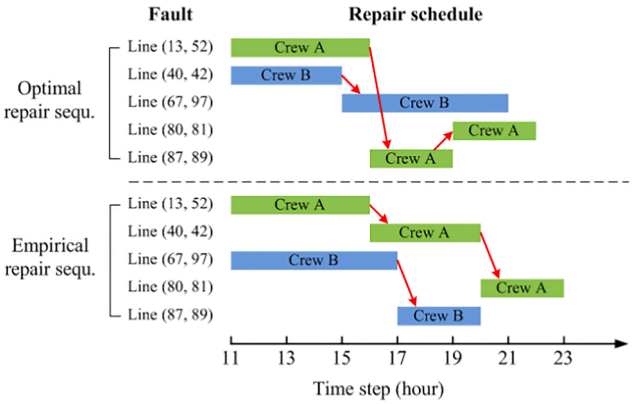

Fig. 16. Repair scheduling of Method 1 and 2.

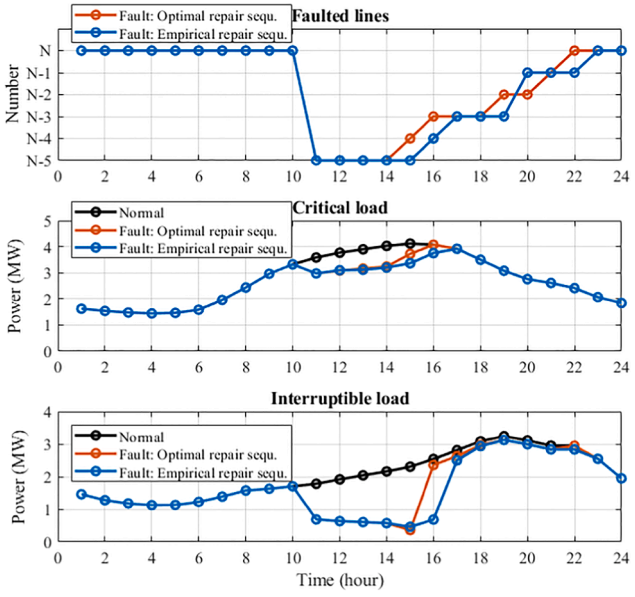

Fig. 17. Progress of line repair and load restoration.

work will focus on the cooperative dispatch of repair crews and mobile energy storage systems for DSRR, as opposed to DERs at fixed locations.

CRediT authorship contribution statement

Qingxin Shi: Conceptualization, Methodology, Formal analysis, Validation, Writing - original draft. **Fangxing Li:** Conceptualization, Methodology, Writing - review & editing, Supervision. **Jin Dong:** Conceptualization, Writing - review & editing. **Mohammed Olama:** Conceptualization, Writing - review & editing. **Xiaofei Wang:** Investigation. **Chris Winstead:** Investigation. **Teja Kuruganti:** Funding acquisition.

Declaration of Competing Interest

The authors declare that they have no known competing financial interests or personal relationships that could have appeared to influence the work reported in this paper.

References

[1] Berkeley AR, et al. A Framework for Establishing Critical Infrastructure Resilience Goals: Final Goals and Recommendations. Washington, DC, USA: Nat. Infrastruct. Advisory Council; Oct. 2010.

[2] Zuloaga S, Vittal V. Quantifying power system operational and infrastructural resilience under extreme conditions within a water-energy nexus framework. IEEE Open Access J Power Energy 2021;8:229–38.

[3] Shi Q, Liu W, Zeng B, Hui H, Li F. Enhancing distribution system resilience against extreme weather events: concept review, algorithm summary, and future vision. Int J Electr Power Energy Syst Jun. 2022;138:1–13.

[4] Drye W, 2017 Hurricane Season Was the Most Expensive in U.S. History. Nat. Geographic., Washington, DC, USA, Nov. 2017. [Online]. Available: https://news.nationalgeographic.com/2017/11/2017-hurricane -season-most-expensive-us-history-spd/.

[5] Arif A, Ma S, et al. Optimizing service restoration in distribution systems with uncertain repair time and demand. IEEE Trans Power Syst Nov. 2018;33(6):6828–38.

[6] Wang Z, Wang J. Self-healing resilient distribution systems based on sectionalization into microgrids. IEEE Trans Power Syst Nov. 2015;30(6):3139–49.

[7] Ding T, Lin Y, Bie Z, Chen C. A resilient microgrid formation strategy for load restoration considering master-slave distributed generators and topology reconfiguration. Appl Energy 2017;199:205–16.

[8] Wang Y, Xu Y, et al. Coordinating multiple sources for service restoration to enhance resilience of distribution systems. IEEE Trans Smart Grid Sep. 2019;10(5):5781–93.

[9] Zhu J, Yuan Y, Wang W. An exact microgrid formation model for load restoration in resilient distribution system. Int J Electric Power Energ Syst Mar. 2020;116:1–9.

[10] Shi Q, Li F, Olama M, Dong J, Xue Y, Starke M, et al. Network reconfiguration and distributed energy resource scheduling for improved distribution system resilience. Int J Electric Power Energ Syst 2021;124:106355. https://doi.org/10.1016/j.ijepes.2020.106355.

[11] Chen B, Chen C, Wang J, Butler-Purry KL. Sequential service restoration for unbalanced distribution systems and microgrids. IEEE Trans Power Syst Mar. 2018;33(2):1507–20.

[12] Chen B, Ye Z, Chen C, Wang J. Toward a MILP modeling framework for distribution system restoration. IEEE Trans Power Syst May 2019;34(3):1749–60.

[13] Arab A, Khodaei A, et al. Stochastic pre-hurricane restoration planning for electric power systems infrastructure. IEEE Trans Smart Grid Mar. 2015;6(2):1046–54.

[14] Esfahani M, Amjady N, et al. Robust resiliency-oriented operation of active distribution networks considering windstorms. IEEE Trans Power Syst Sep. 2020;35(5):3481–93.

[15] Tan Y, Qiu F, et al. Scheduling post-disaster repairs in electricity distribution networks. IEEE Trans Power Syst Jul. 2019;34(4):2611–21.

[16] Arif A, Wang Z, et al. Power distribution system outage management with co-optimization of repairs, reconfiguration, and DG dispatch. IEEE Trans Smart Grid Sep. 2018;9(5):4109–18.

[17] Arif A, Wang Z, Chen C, Wang J. Repair and resource scheduling in unbalanced distribution systems using neighborhood search. IEEE Trans Smart Grid 2020;11(1):673–85.

[20] Gade D, Hackebeil G, Ryan SM, Watson J-P, Wets R-B, Woodruff DL. Obtaining lower bounds from the progressive hedging algorithm for stochastic mixed-integer programs. Math Program 2016;157(1):47–67.

[21] Linderoth J, Shapiro A, Wright S. The empirical behavior of sampling methods for stochastic programming. Ann Oper Res 2006;142(1):215–41.

[22] Hurricanes in history, National hurricane center and central Pacific Hurricane center. Available: https://www.nhc.noaa.gov/outreach/history/.

[23] Dehghani NL, Jeddi AB, Shafieezadeh A. Intelligent hurricane resilience enhancement of power distribution systems via deep reinforcement learning. Appl Energy 2021;285:116355. https://doi.org/10.1016/j.apenergy.2020.116355.

[24] Das Y. Parametric modeling of tropical cyclone wind fields in India. Nat Hazards Sep. 2018;93:1049–84.

[25] Campbell RJ. Weather-Related Power Outages and Electric System Resiliency: Congressional Research Service. Washington, DC, USA: Library of Congress; 2012.

[26] Distribution system automation: Results from the smart grid investment grant program, Dept. of Energy, Sep. 2016. [Available] https://www.energy.gov/sites/prod/files/2016/11/f34/Distribution%20Automation%20Summary%20Report_09-29-16.pdf.

[27] Wei W, Wu D, Wang Z, Mei S, Catalao JPS. Impact of energy storage on economic dispatch of distribution systems: a multi-parametric linear programming approach and its implications. IEEE Open Access J Power Energy 2020;7:243–53.

[28] Chen L, Wang J, Wu Z, Li G, Zhou M, Li P, et al. Communication reliability-restricted energy sharing strategy in active distribution networks. Appl Energy 2021;282:116238. https://doi.org/10.1016/j.apenergy.2020.116238.

[29] Arab A, Khodaei A, Han Z, Khator SK. Proactive recovery of electric power assets for resiliency enhancement. IEEE Access Feb. 2015;3:99–109.

[30] Jaech A, Zhang B, Ostendorf M, Kirschen DS. Real-time prediction of the duration of distribution system outages. IEEE Trans Power Syst 2019;34(1):773–81.

[31] Lei S, Chen C, Zhou H, Hou Y. Routing and scheduling of mobile power sources for distribution system resilience enhancement. IEEE Trans Smart Grid Sep. 2019;10(5):5650–62.

[32] Hao J, Gao DW, Zhang JJ. Reinforcement learning for building energy optimization through controlling of central HVAC system. IEEE Open Access J Power Energy 2020;7:320–8.

[33] Balakrishnan R, Ranganathan K. A textbook of graph theory. Springer; 2012. p. 75.

[34] Electricity storage and renewables: cost and market to 2030, International Renewable Energy Agency (IRENA), Oct 2017.

[35] Koohi-Fayegh S, Rosen MA. A review of energy storage types, applications and recent developments. J Energy Storage Feb. 2020;27:1–23.

[36] Chen C, Wang J, Qiu F, Zhao D. Resilient distribution system by microgrids formation after natural Disasters. IEEE Trans Smart Grid 2016;7(2):958–66.